Temperature-dependent pinning of vortices in low-angle grain boundaries in $YBa_2Cu_3O_{7-\delta}$

J. Albrecht
Max-Planck-Institut für Metallforschung, Heisenbergstrasse 3, D-70569 Stuttgart, Germany
and Max-Planck-Institut für Festkörperforschung, Heisenbergstrasse 1, D-70569 Stuttgart, Germany
(Received 16 December 2002; revised manuscript received 14 May 2003; published 6 August 2003)

Low-angle grain boundaries with misorientation angles $\theta<5°$ in optimally doped thin films of $YBa_2Cu_3O_{7-\delta}$ are investigated by magneto-optical imaging. With a numerical inversion scheme of Biot-Savart's law it is possible to obtain the critical current density across the grain boundary with a spatial resolution of about 5 μm. This technique is now applied to determine the temperature dependence of the critical current density across low-angle grain boundaries. The detailed analysis of the temperature dependence shows a crossover in the pinning properties of Abrikosov-Josephson vortices which are located in the grain boundary.

DOI: 10.1103/PhysRevB.68.054508 PACS number(s): 74.25.Sv, 74.72.Bk, 74.78.Bz, 74.25.Qt

The critical current density in thin epitaxial films of high-temperature superconductors of up to $j_c=8\times10^{11}$ A/m^2 at a temperature of $T=5$ K has its origin in the efficient pinning of flux lines.[1,2] In the case of films on well oriented, unmodified substrates, screw dislocations,[3] edge dislocations,[4] dislocation chains,[5] or columnar defects[6] are discussed as pinning sites, mainly generated due to growth mode associated effects and/or the relaxation of the film stress caused by the lattice mismatch to the substrate. The presence of grain boundaries, however, drastically reduces the critical currents of these films. At the grain boundary, the local breaking of the crystal symmetry causes an array of dislocation cores in the superconducting film. The strain field of these dislocations creates regularly ordered normal conducting regions.[7–9] Although the superconductivity is suppressed at these dislocations, these normal conducting regions can act as pinning sites for flux lines.[10] It has been found that the critical current across grain boundaries decreases exponentially with increasing misorientation angle above a threshold angle of $\theta_c \approx 5°$.[11–15] An explanation can be given by a local bending of the band structure[16,17] in combination with the appearance of localized states due to oxygen deficiency or disorder.[18–20] The behavior of the critical current across grain boundaries with misorientation angles lower than θ_c is found to be very complex,[21,22] the critical current strongly depends on the relative orientation of the grain boundary to the current flow[23] and on the local magnetic-flux density.[24] Therefore, this topic is still the subject of intense research.

In this paper, detailed investigations of current densities across low-angle grain boundaries are presented, with particular stress on the temperature dependence of the critical current. The measurements show a distinct difference between the temperature dependence of the current densities across the grain boundary and the current densities in the adjacent grains. This is strongly related to the different structure of the flux lines in and between the grains.[25,26] With the application of a quantitative magneto-optical technique, it is now possible measure the critical current density across low-angle grain boundaries with a spatial resolution of a few micrometers. This resolution is adequate to extract the part of the critical current that is not related to flux line interactions with neighboring vortices[24] and can therefore be used to investigate the pinning that acts on the so-called Abrikosov-Josephson (AJ) vortices inside the grain boundary.[26,27]

The experiments are carried out on thin films of optimally doped $YBa_2Cu_3O_{7-\delta}$ (YBCO) grown on bicrystalline strontium titanate substrates. The substrates are oriented in [001] direction and contain symmetric tilt grain boundaries with misorientation angles of 0°–5°. The YBCO films are grown by pulsed laser deposition up to a thickness of typically 150 nm. Afterwards a chemical etching process is performed to obtain square shaped films with a lateral dimension of 1 mm.

The critical currents of the grain boundaries are measured by means of quantitative magneto-optics in the temperature range of $T=7-90$ K. The experimental setup consists of a ferrimagnetic lutetium-doped iron garnet film as field sensing layer[28] and combination of a polarization light microscope and a charge-coupled device camera. The magnetic-flux density distribution can be imaged with a spatial resolution of about 3 μm with high quantitative precission.[29]

Figure 1 shows the magneto-optical image of a YBCO film containing a 3° boundary at different temperatures. The gray-scale represents the flux density component B_z perpendicular to the film, bright parts refer to high local flux densities. The images are obtained after zero-field cooling and applying an external field at temperatures of $T=7$, 25, and 50 K. The magnitude of the external field is chosen with the criterion to observe a constant penetration depth in the unperturbed film for all temperatures. This lead to external fields of $B_{ex}=48,32,16$ mT, respectively. The influence of the grain boundary occurs as the two bright lines in the upper part of the images.

These measurements show a changing influence of the grain boundary on the flux density distribution at different temperatures. Whereas the penetration depth in the unperturbed film is nearly constant as mentioned above, a strong increase of the penetration depth at the grain boundary with increasing temperature can be observed. This is directly related to a significant drop of the grain-boundary current with respect to the film current.

To get deeper insight into the current-density distribution the magnetic-flux density data are treated by a numerical calculation scheme. The calculus is based on the law of Biot

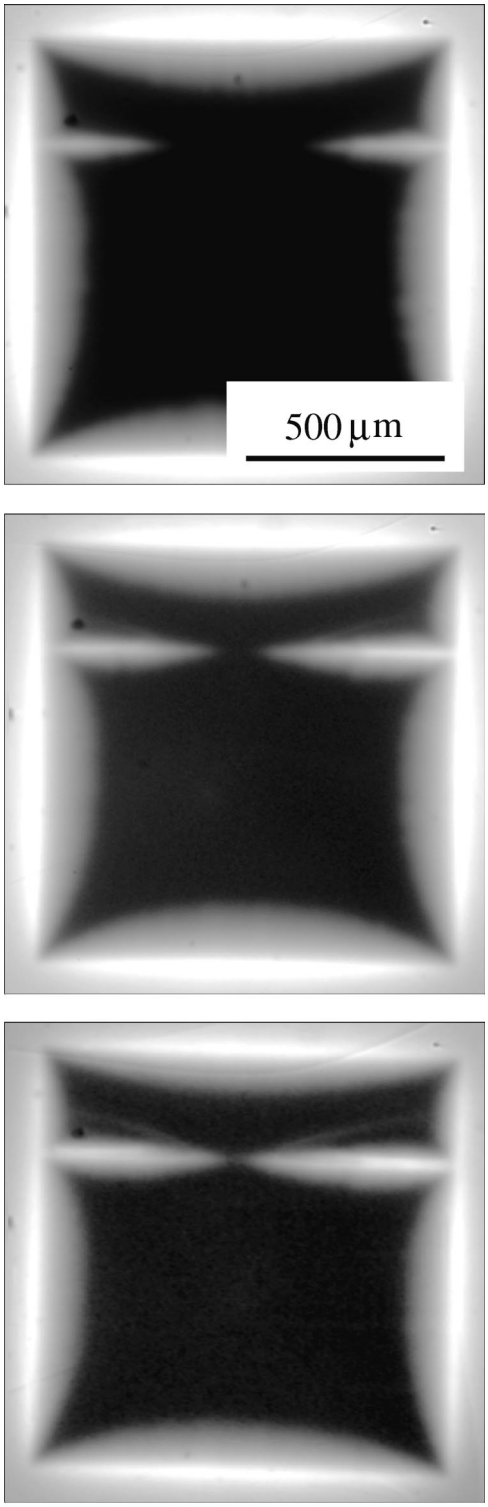

FIG. 1. Magneto-optical images of the flux density distribution of the bicrystalline sample containing a symmetric 3° grain boundary at different temperatures: $T=7$ K (top), $T=25$ K (middle), $T=50$ K (bottom). The applied external fields are 48 mT, 32 mT, and 16 mT, respectively.

and Savart that relates the flux density distribution with the current density appearing in the sample. For the case of a two-dimensional current-density distribution $\mathbf{j}=(j_x,j_y,0)$, it reads explicitly

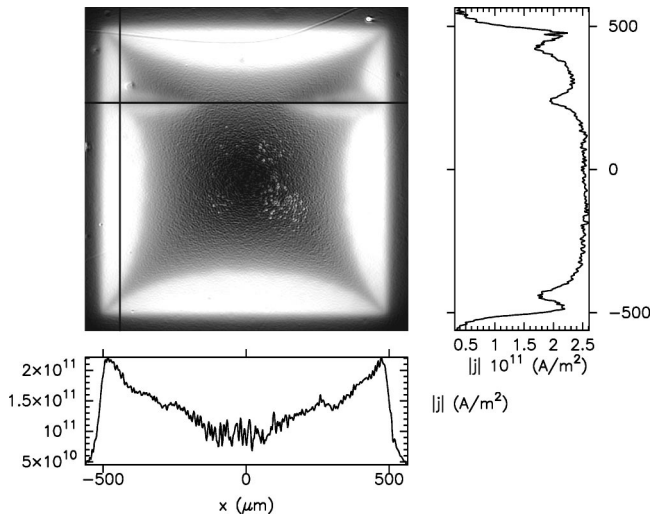

FIG. 2. Magnitude of the current density in the YBCO film containing a 3° grain boundary at $T=7$ K. White parts of the gray-scale representation refer to a current density $j=2.5\times10^{11}$ A/m^2. The profiles on the left and below the image refer to the current density along the solid black lines.

$$B_z(x,y)=\mu_0 H_{ex} + \mu_0\int_V \frac{j_x(\mathbf{r}')(y-y')-j_y(\mathbf{r}')(x-x')}{4\pi|\mathbf{r}-\mathbf{r}'|^3}d^3r'. \tag{1}$$

For this special case, this relation can be inverted unambiguously by using Fourier transformation and the convolution theorem.[30] The application of this numerical scheme allows the calculation of the current-density distribution in the sample with a lateral resolution of about 5 μm. The reduction of the resolution compared to the flux density measurement is due to a necessary suppression of the experimental noise level which is enhanced by the Fourier-transform procedure.

The application of the inversion scheme on the data of Fig. 1 yields the corresponding current-density distribution. A gray-scale representation of the magnitude of the current density for the measurement at $T=5$ K is plotted in Fig. 2.

The horizontal profile in Fig. 2 indicates the current density that crosses the grain boundary. In contrast to the current density occurring in the unperturbed film, which has a constant magnitude of $j_c\approx2.5\times10^{11}$ A/m^2, the grain-boundary current density varies drastically. This is related to the strong dependence of the grain-boundary current on the local magnetic-flux density.[31] A strong increase of the grain-boundary current density with increasing local flux density can be found in low-angle grain boundaries. This is related to the influence of vortex-vortex interactions inside and in the vicinity of the grain boundary.[24]

To obtain information about the structure of the grain-boundary vortices, the interaction between the flux lines and the grain-boundary dislocations is of high interest. To extract this interaction from the current-density data, it is necessary to get rid of the influence of vortex-vortex interactions. This

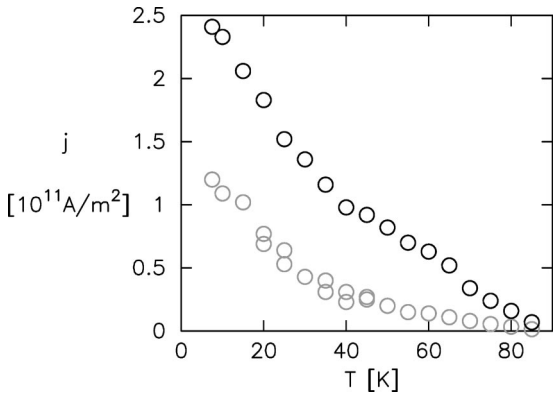

FIG. 3. Temperature dependence of the critical current densities across the grain-boundary (gray) and in the grains (black).

can be done by focussing the determination of the current density on selected sections of the grain boundaries, where the influence of the magnetic-flux density is small. For this purpose, two main conditions have to be taken into account: First, the local magnetic-flux density at the measured section has to be small enough to reduce the vortex-vortex interactions and second, it is necessary to have the grains in this section already penetrated by magnetic flux to avoid perturbing surface barrier effects.[29] These conditions are, of course, temperature dependent and it has been found that a local flux density of $B_{loc}=(1/2)B_{1/3}$ is suitable, with $B_{1/3}$ giving the external flux density that leads to a penetration depth of about 1/3 of the distance between the samples border and center. This refers to the situation that is shown in Figs. 1(a–c) and leads, e.g., to $B_{loc}\approx 16$ mT at $T=25$ K. Even if the magnitude of the local flux density is small, it is necessary to subtract the influence of the local flux line-flux line interaction on the current density, this is done by assuming a model which is presented in Albrecht *et al.*[24]

Under the above conditions the temperature dependence of the critical current on the 3° boundary is determined. Figure 3 shows the current densities of the unperturbed film and the grain-boundary in the temperature range of $T=7-90$ K.

Apart from the fact that there is a difference by a factor of about 2 between the two current densities, no significant feature of the grain-boundary current can be observed in Fig. 3. To get a deeper insight into the temperature dependence, a power-law behavior $j\propto(T_c-T)^{-\alpha}$ is checked by plotting the data on a logarithmic scale over $(T_c-T)^{-1}$. The Ginzburg-Landau power-law dependences of the two characteristic length scales $\lambda,\xi\propto(T_c-T)^{-1/2}$ suggest this ansatz.

Figures 4 and 5 show the temperature-dependent current densities across the grain-boundary and in the grains on the introduced logarithmic scale.

The current-density data in Fig. 4 can be described by a two-step power-law behavior. In the temperature range between $T=7$ K and about 38 K, the phenomenological description $j(T)\propto(T-T_c)^{-\alpha}$ yields an exponent $\alpha=1.7$, which is depicted by the straight line (a) in Fig. 4. For higher temperatures, the slope of the fitting curve changes and one finds $\alpha=1.0$ [straight line (b)]. This result is now compared

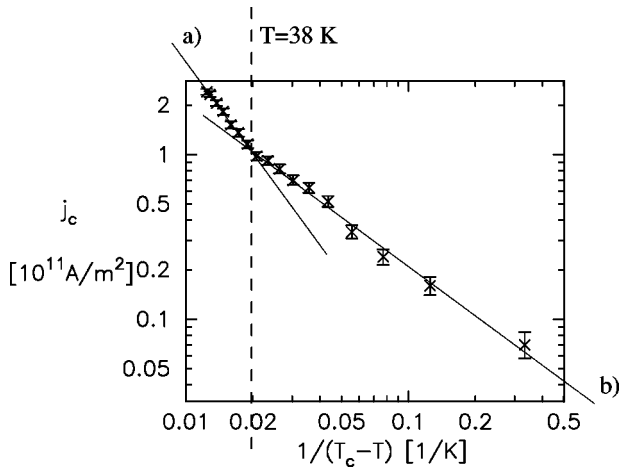

FIG. 4. Logarithmic plot of the current density in the grains. The lines represent a power-law behavior $j_b\propto(T_c-T)^{-\alpha}$ for $\alpha=1.7$ (a) and $\alpha=1.0$ (b).

with the temperature-dependent set of data for the grain-boundary. This is shown in Fig. 5.

For the grain-boundary current density also a two-step behavior is found. The crossover temperature is determined with $T\approx 44$ K, which is in the same range as in the case of the film current. In the temperature regime below the crossover, the exponent α is found to be $\alpha=3.0$, a much stronger decrease than the current density in the film shows. This explains again the magnetic flux penetration in the magneto-optical images of Fig. 1. For higher temperature, the slope of the fitting straight line also changes. In the higher-temperature range above $T=44$ K with $\alpha=1.1$ nearly the same power-law dependence occurs as found for the current density in the grains.

To obtain further information another sample also containing a symmetric 3° tilt grain-boundary is investigated, this time in the remanent state. An external field of $B_{ex}=250$ mT has been applied, afterwards the measurement is performed in zero field. This sample shows a current density in the banks of $j_c=3.0\times10^{11}$ A/m^2 at $T=7$ K, a slightly

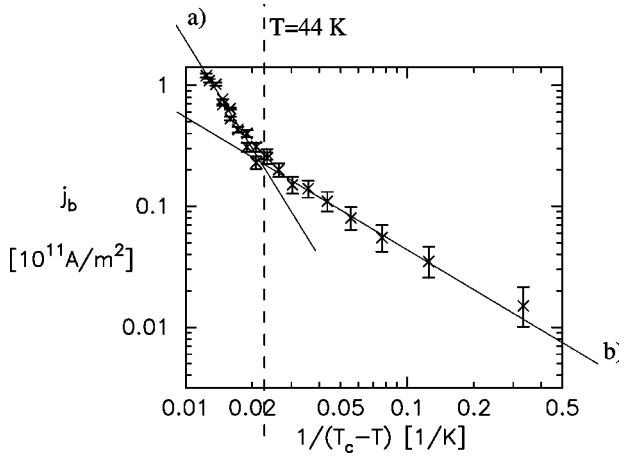

FIG. 5. Logarithmic plot of the grain-boundary current density. The lines represent a power-law behavior $j_b\propto(T_c-T)^{-\alpha}$ for $\alpha=3.0$ (a) and $\alpha=1.1$ (b).

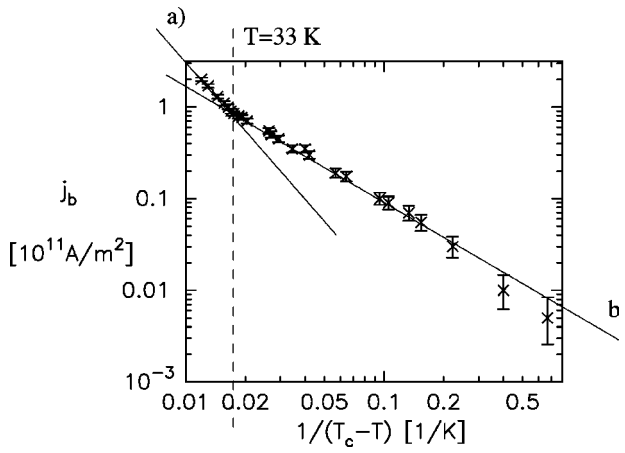

FIG. 6. Logarithmic plot of the current density of a different sample measured in the remanent state. The lines give the power-law behavior $j_b \propto (T_c-T)^{-\alpha}$ with $\alpha=2.5$ (a) and $\alpha=1.2$ (b).

higher value than the sample before. The grain-boundary current density is determined in this case in the remanent state of the sample. In the remanent state there is always a position, where the local flux density is zero, which means that the current density at this point is only determined by the pinning of the vortices at the grain-boundary dislocations. The temperature dependence of the current density at this point is depicted in Fig. 6.

It is found that the grain-boundary currents are slightly higher compared to the measurement in Fig. 5, which can be related to the generally higher current density of the sample or to an improved microstructure of the grain-boundary. A power-law fit of the data at low temperatures, gives a value of the exponent $\alpha=2.5$. In case of higher temperatures, an exponent $\alpha=1.2$ is found which is again in the same range as the values found from the measurements depicted in Figs. 4 and 5. The deviation from the power-law behavior that occurs for the data points very close to T_c is originated in the error bar concerning the determination of T_c. However, this affects only the two data points at high temperatures which are not very robust against the determination of T_c. This does not influence the value of α at all.

These surprising results will now be discussed in the following. The faster decrease of the grain-boundary currents with increasing temperature below $T=30-40$ K can be understood by considering the pinning scenarios that are responsible for the current densities. The current density in thin films of high-temperature superconductors is determined by the pinning of flux lines at defect structures with feasible lateral dimensions. The predominant pinning mechanism is flux-line core pinning. The condensation energy of a flux line per unit length $\epsilon=\Phi_0^2/(4\pi\mu_0\lambda^2)$ can vary on the length scale of the coherence length ξ, which is given in the framework of Ginzburg-Landau theory by $\xi=\xi_0(T_c-T)^{1/2}$ and $\xi_0\approx 1.2$ nm for the case of YBCO.[33] The presence of a defect with a radius L in the film now introduces a local variation of ϵ_0. The resulting pinning force density $f_{pin}=\max[\partial\epsilon/\partial x]$ can be estimated by $f_{pin}\approx\delta\epsilon/L$, with δ giving the reduction of ϵ_0, always under the restriction $L\geqslant\xi$. This relation clearly shows that the pinning force density decreases with increasing defect radii L and increasing coherence length ξ. At the same time, it can be seen that a defect size that equals the coherence length ξ shows maximum pinning force density. Owing to the temperature dependence of ξ, there are different effective pinning sites at different temperatures.

To obtain insight into the occurring temperature dependences, we consider first the Ginzburg-Landau solution for the penetration depth $\lambda=\lambda_0(T_c-T)^{1/2}$, with $\lambda_0\approx 130$ nm for YBCO.[34,35] The condensation energy ϵ is in first-order approximation proportional to λ^{-2}, which gives rise to a temperature dependence of $\epsilon(T)=\epsilon_0(T_c-T)^{-1}$. The fact that the most effective pinning sites change with temperature leads to the approximation that the critical current density is proportional to the condensation energy ϵ, this suggests $j_c \propto (T_c-T)^{-1}$ or $\alpha=1$, respectively.

The understanding of the measured temperature dependences requires a more detailed consideration of the pinning properties of the flux lines in the grain-boundary and in the banks. The vortices in the banks are isotropic Abrikosov vortices that are pinned at structural defects in the film. The high current density results from the fact that there are existing defects with structural dimensions comparable to the coherence length ξ which allow nearly optimum pinning and lead to the high occurring current densities of more than $j_c=2\times 10^{11}$ A/m^2. In the presented measurements, the flux-line density is always much lower than the defect density, so the flux lines occupy only the most effective pinning sites.

In the case of a symmetric 3° tilt grain-boundary, the vortices in the grain-boundary are AJ vortices.[27] These vortices have an enlarged coherence length $\xi_b \gg \xi$ along the grain-boundary and therefore an anisotropic vortex core. The grain boundary itself can be characterized by an array of edge dislocations with nonsuperconducting dislocation cores.[32] In the case of a 3° grain boundary, these dislocations have a distance of about $d=7-8$ nm. These dislocations act as pinning centers for the AJ vortices and give rise to large current densities across low-angle grain boundaries.[10]

With this knowledge it is possible to understand the different temperature dependence of the film and the grain-boundary current in the low-temperature regime. The anisotropic AJ vortices in the grain boundary are pinned at the nonsuperconducting dislocation cores of the edge dislocations located in the grain boundary. With increasing temperature the condensation energy of the flux lines is reduced, additionally the pinning potential of the dislocations is weakened, because the lateral dimension of the nonsuperconducting dislocation cores increases.[25] This leads to a stronger decrease of the grain-boundary currents as compared to the film currents. The isotropic Abrikosov vortices in the film are located in a landscape of defects with varying lateral dimensions. Owing to the fact that the pinning force density has a maximum when the coherence length and the defect size match, the flux lines can always find a potential depth which shows feasible pinning features. This reduces strongly the temperature-dependent decay of the current density. Therefore, the current-density decrease in the film is much weaker than in the grain-boundary. The smaller exponent $\alpha=2.5$, which is found for the second sample, is related to the higher

current density across the grain boundary. This means in this picture that the grain-boundary vortices in this sample are less anisotropic.

With the above described scenario one is able to understand the temperature dependence of the critical current densities of film and grain boundary in the temperature region below $T=30-40$ K. Above this temperature both experimental sets of data show a different behavior of the current density. It can be found $j_c \propto (T_c - T)^{-\alpha}$ with $\alpha \approx 1.0-1.2$ for all of the current-temperature curves. A change in the pinning properties occurs above which the different scenarios show the same temperature dependence but with a different magnitude of the current density. Gurevich *et al.*[36] suggested that AJ vortices in low-angle grain boundaries should become more anisotropic with increasing temperature, this means that the decay of the current density at higher temperatures should become faster. This cannot be found in the data presented in this paper. Furthermore, a weaker decay of the grain-boundary current is measured in the temperature range between $T=40-90$ K.

Additionally, the same exponent of the power-law behavior for both the film and the grain-boundary currents is found at higher temperatures. Bringmann *et al.*[37] showed that the presence of defect structures in vicinity of the grain-boundary can lead to a more complex shape of the AJ vortices. The current data of the Figs. 4 –6 now suggest that those vortices with a complex core geometry show a very similar pinning behavior as the isotropic Abrikosov vortices in the banks, only with an enhanced averaged core size that leads to a reduction of the current magnitude. This approach explains the same temperature dependence of the curves in Figs. 4–6, respectively.

In conclusion, it is found that the quantitative magneto-optical Faraday effect is an excellent tool to investigate the local current transport in thin films of high-temperature superconductors. The local relation between magnetic flux and current density can be determined and with this knowledge it is possible to separate the different origins of the pinning force density, namely, the vortex-microstructure and the vortex-vortex interaction. The consideration of the pinning force density and therefore the critical current density which is caused by the microstructural pinning of vortices shows that both the film currents and the grain-boundary currents have different origins in different temperature regimes. In case of the grain-boundary current, the description of anisotropic elongated Abrikosov-Josephson vortices which are pinned at edge dislocations in the grain-boundary are not feasible for the whole temperature range between $T=7$ K and T_c. At higher temperatures, the grain-boundary vortices are pinned in a very similar way as the isotropic Abrikosov vortices are, this can be clearly proved by the measured temperature dependence.

The author is grateful to Ch. Jooss, E. H. Brandt, S. Leonhardt, H.–U. Habermeier, and H. Kronmüller for stimulating and helpful discussions and to G. Cristiani and H.–U. Habermeier for the preparation of the excellent samples.

[1] B. Dam, J.M. Huijbregtse, F.C. Klaasen, R.C.F. van der Geest, G. Doornbos, J.H. Rector, A.M. Testa, S. Freisem, J.C. Martinez, B. Stäuble-Pümpin, and R. Griessen, Nature (London) **399**, 439 (1999).

[2] Ch. Jooss, R. Warthmann, and H. Kronmüller, Phys. Rev. B **61**, 12 433 (2000).

[3] J. Mannhart, D. Anselmetti, J.G. Bednorz, A. Catana, Ch. Gerber, K.A. Müller, and D.G. Schlom, Z. Phys. B: Condens. Matter **86**, 177 (1992).

[4] J.M. Huijbregtse, B. Dam, R.C.F. van der Geest, F.C. Klaassen, R. Elberse, J.H. Rector, and R. Griessen, Phys. Rev. B **62**, 1338 (2000).

[5] R.M. Schalk, K. Kundzins, H.W. Weber, E. Stangl, S. Proyer, and D. Bäuerle, Physica C **257**, 341 (1996).

[6] L. Civale, A.D. Marwick, T.K. Worthington, M.A. Kirk, J.R. Thompson, L. Krusin-Elbaum, Y. Sun, J.R. Clem, and F. Holtzberg, Phys. Rev. Lett. **67**, 648 (1991).

[7] J.B. Hirth and J. Lothe, *Theory of Dislocations* (McGraw-Hill, New York, 1968).

[8] A.P. Sutton and R.W. Balluffi, *Interfaces in Crystalline Materials* (Clarendon, Oxford, 1995).

[9] J.A. Alarco and E. Olsson, Phys. Rev. B **52**, 13 625 (1995).

[10] A. Diaz, L. Mechin, P. Berghuis, and J.E. Evetts, Phys. Rev. Lett. **80**, 3855 (1998).

[11] D. Dimos, P. Chaudhari, J. Mannhart, and F.K. LeGoues, Phys. Rev. Lett. **61**, 219 (1988).

[12] M.F. Chisholm and M.F. Pennycook, Nature (London) **351**, 47 (1991).

[13] R. Gross, in *Interfaces in High-T_c Superconducting Systems*, edited by S.L. Shinde and D.A. Rudman (Springer-Verlag, New York, 1994), p. 176.

[14] A.A. Polyanskii, A. Gurevich, A.E. Pashitski, N.F. Heinig, R.D. Redwing, J.E. Nordman, and D.C. Larbalestier, Phys. Rev. B **53**, 8687 (1996).

[15] H. Hilgenkamp, J. Mannhart, and B. Mayer, Phys. Rev. B **53**, 14 586 (1996).

[16] J. Mannhart and H. Hilgenkamp, Supercond. Sci. Technol. **10**, 880 (1997).

[17] H. Hilgenkamp and J. Mannhart, Appl. Phys. Lett. **73**, 265 (1998).

[18] R. Gross and B. Mayer, Physica C **180**, 235 (1991).

[19] J. Halbritter, Phys. Rev. B **46**, 14 861 (1992).

[20] B.H. Moeckly, D.K. Lathrop, and R.A. Buhrman, Phys. Rev. B **47**, 400 (1993).

[21] Z.G. Ivanov, P.A. Nilsson, D. Winkler, J.A. Alarco, T. Claeson, E.A. Stepantsov, and A.Ya. Tzalenchuk, Appl. Phys. Lett. **59**, 3030 (1991).

[22] N.F. Heinig, R.D. Redwing, J.E. Nordman, and D.C. Larbalestier, Phys. Rev. B **60**, 1409 (1999).

[23] Ch. Jooss and J. Albrecht, Z. Metallkd. **93**, 1065 (2002).

[24] J. Albrecht, S. Leonhardt, and H. Kronmüller, Phys. Rev. B **63**, 014507 (2001).

[25] A. Gurevich and E.A. Pashitskii, Phys. Rev. B **57**, 13 878 (1998).
[26] A. Gurevich, Phys. Rev. B **65**, 214531 (2002).
[27] A. Gurevich, Phys. Rev. B **48**, 12 857 (1993).
[28] L.A. Dorosinskii, M.V. Indenbom, V.A. Nikitenko, Yu.A. Ossip'yan, A.A. Polyanskii, and V.K. Vlasko-Vlasov, Physica C **203**, 149 (1992).
[29] Ch. Jooss, J. Albrecht, H. Kuhn, S. Leonhardt, and H. Kronmüller, Rep. Prog. Phys. **65**, 651 (2002).
[30] Ch. Jooss, R. Warthmann, A. Forkl, and H. Kronmüller, Physica C **299**, 215 (1998).
[31] J. Albrecht, R. Warthmann, S. Leonhardt, and H. Kronmüller, Physica C **341–348**, 1459 (2000).
[32] A. Gurevich and L.D. Cooley, Phys. Rev. B **50**, 13 563 (1994).
[33] K. Winzer and G. Kumm, Z. Phys. B: Condens. Matter **82**, 317 (1991).
[34] D.N. Basov, R. Liang, D.A. Bonn, W.N. Hardy, B. Dabrowski, M. Quijada, D.B. Tanner, J.P. Rice, D.M. Ginsberg, and T. Timusk, Phys. Rev. Lett. **74**, 598 (1995).
[35] J.L. Tallon, C. Bernhard, U. Binninger, A. Hofer, G.V.M. Williams, E.J. Ansaldo, J.I. Budnick, and Ch. Niedermayer, Phys. Rev. Lett. **74**, 1008 (1995).
[36] A. Gurevich, M.S. Rzchowski, G. Daniels, S. Patnaik, B.M. Hinaus, F. Carillo, F. Tafuri, and D.C. Larbalestier, Phys. Rev. Lett. **88**, 097001 (2002).
[37] B. Bringmann, H. Walter, Ch. Jooss, A. Leenders, and H.C. Freyhardt, Physica C **372–376**, 1478 (2002).